

Assessing the Feasibility of Using Deformable Registration for On-board Multi-modality  
Based Target Localization in Radiation Therapy

by

Ge Ren

Graduate Program in Medical Physics  
Duke Kunshan University and Duke University

Date: \_\_\_\_\_

Approved:

\_\_\_\_\_  
Lei Ren, Supervisor

\_\_\_\_\_  
Fang-Fang Yin

\_\_\_\_\_  
David Huang

Thesis submitted in partial fulfillment of  
the requirements for the degree of  
Master of Science in the  
Medical Physics in the Graduate School  
of Duke Kunshan University and Duke University

2018

ABSTRACT

Assessing the Feasibility of Using Deformable Registration for On-board Multi-modality

Based Target Localization in Radiation Therapy

by

Ge Ren

Graduate Program in Medical Physics  
Duke Kunshan University and Duke University

Date: \_\_\_\_\_

Approved:

\_\_\_\_\_  
Lei Ren, Supervisor

\_\_\_\_\_  
Fang-Fang Yin

\_\_\_\_\_  
David Huang

An abstract of a thesis submitted in partial fulfillment of  
the requirements for the degree of  
Master of Science in the  
Medical Physics in the Graduate School  
of Duke Kunshan University and Duke University

2018

Copyright by  
Ge Ren  
2018

## **Abstract**

### **Purpose:**

Cone beam computed tomography (CBCT) is typically used for on-board target localization in radiation therapy. However, CBCT has poor soft tissue contrast, which makes it extremely challenging to localize tumors in soft tissues such as liver, prostate and breast cancers. This study explores the feasibility of using prior images and deformable image registration (DIR) to generate on-board multi-modality images to improve the soft tissue contrast for target localization in radiation therapy.

### **Methods:**

Patient CT or MR images are acquired during the simulation stage and are used as the prior images. CBCT images are acquired on-board for clinical target localization. B-spline based deformable registration is used to register MR or CT images with CBCT images to generate synthetic on-board MR/CT images, which are used for on-board target localization. Liver, prostate, and breast patient data were used in the study to investigate the feasibility of the method. The evaluation includes three aims: (1). Evaluate whether the rigid registration and margin design in current clinical practice is sufficient to ensure the coverage of the on-board tumor volume: the synthetic on-board MR/CT images are used to verify the target coverage based on the shifts determined by CT-CBCT rigid body registration in clinical practice; (2). Evaluate the potential for

margin optimization based on the synthetic on-board multi-modality imaging technique: shifts are determined by rigid registration between planning CT and synthetic on-board MR/CT, and the minimal PTV margin is determined to ensure coverage of the deformed tumor volume; (3). Evaluate the effects of hypothetical DIR uncertainty on the margin optimization: different hypothetical DIR uncertainties were added as extra margins to the deformed margin as the correspondence evaluated margin response obtained from aim 2 to investigate their effects on the final margin design.

### **Results:**

In the process of DIR, using CT images as the prior images for soft tissue deformable registration showed a better alignment of the boundary than using MRI as the prior images. The evaluation showed: (1). Most of the tumor volume defined by the on-board synthetic images was covered by the PTV based on the shifts applied in clinical practice. For the liver cases, the coverage of 6 in 8 cases is above 90%. For the breast cases, the coverage of 6 in 7 cases is above 90%. For the prostate, the coverage of all cases is above 94%. The under-dosed cases are correlated with larger interfraction deformation in long treatment course, small tumor volume, and insufficient PTV margin. (2). For 6 of the liver cases, 5 of the prostate cases, and all the breast cases, the synthetic images allowed the reduction of PTV margin to 1.5-7 mm, 1-4 mm, and 1 -1.5 mm, respectively. For the cases with reduced optimized margin, the dose to the normal tissue can be reduced based on the optimized margin. For the cases with increased

optimized margin the dose to the normal tissue was modestly increased. (3). The hypothetical DIR uncertainties that still led to reduce final PTV margins were 2-4 mm, 1-5mm, and 2-3 mm for liver, prostate, and breast cases respectively. Compared to the conventional imaging and margin design, the proposed method ensures the adequate coverage of the tumor volume while reducing the PTV margin for some patients.

**Conclusion:**

Our studies demonstrated the feasibilities of using on-board synthetic multi-modality imaging to improve the soft tissue contrast for target localization in low contrast regions. This new technique holds great promises to optimize the PTV margin and improve the treatment accuracy.

# Contents

Abstract .....	iv
List of Tables.....	x
List of Figures .....	xi
Acknowledgements .....	xiii
1. Introduction and Background .....	1
1.1 General workflow of radiation therapy .....	1
1.2 Challenges in soft tissue target localization.....	3
1.2.1 Limited soft tissue contrast in CBCT.....	3
1.2.2 Patient setup variations.....	5
1.3 Deformable image registration (DIR) .....	7
1.3.1 Image registration in radiation therapy .....	7
1.3.2 Brief introduction of deformable image registration (DIR).....	8
1.4 Research aim .....	10
2. Materials and Methods.....	11
2.1 Generation of on-board multi-modality images.....	11
2.1.1 Image acquisition .....	11
2.1.2 Deformable image registration.....	12
2.1.3 Assessing the quality of DIR.....	13
2.2 Evaluation of the feasibility of the DIR based target localization .....	13
2.2.1 Evaluation of the deformed CTV coverage in clinical practice.....	14

2.2.2 Evaluation of the potential to optimize the PTV margin and dosimetric effect .....	15
2.2.2.1 Equivalent volume margin(EVM) .....	15
2.2.2.2 Optimization of the CTV/ITV to PTV margin.....	16
2.2.2.3 Evaluation of the dosimetric effects .....	17
2.2.3 Evaluation of the hypothetical margin to account for uncertainties in DIR .....	17
3. Results.....	19
3.1 DIR quality comparison of using CT/MR as the prior images.....	19
3.2. Results of the coverage of the CTV based on clinical shifts .....	22
3.3 Evaluation of the potential to optimize the PTV margin and dosimetric effect....	26
3.3.1 Equivalent volume margin(EVM) and multi-modality margin .....	26
3.3.2 Dosimetric evaluation.....	28
3.3.2.1 Dosimetric evaluation of the liver SBRT cases.....	28
3.3.2.2 Dosimetric evaluation of the prostate cases .....	32
3.3.2.3 Dosimetric evaluation of the breast case .....	34
3.4 Results of the evaluation of the hypothetical DIR uncertainty margin .....	36
4. Discussion.....	38
4.1 Comparison of the MRI-based and CT images based deformable image registration .....	38
4.2 Evaluation of the coverage based on the clinical practice .....	39
4.3 The optimization of the margin and the dosimetric effect .....	40
4.4 Margin optimization based on hypothetical DIR uncertainty .....	41
4.5 Limitations of the study.....	42

5. Conclusion .....	43
Reference .....	44

## List of Tables

Table 1 Coverage of the deformed tumor volume based on clinical shifts for liver patients .....	22
Table 2 Coverage of the deformed tumor volume based on clinical shifts for prostate patients .....	24
Table 3 Coverage of the deformed tumor volume based on clinical shifts for breast patients .....	24
Table 4 Dosimetric comparison of the original plan and optimized plan for liver cases with reduced margin .....	29
Table 5 Dosimetric comparison of the original plan and optimized plan for liver cases with increased margin.....	30
Table 6 Dosimetric comparisons of the original plan and new plan for the prostate cases with reduced margin .....	32
Table 7 Dosimetric comparison of the original plan and optimized plan for prostate patients with increased margin.....	33
Table 8 Dosimetric comparison of the original plan and optimized plan for the breast cases with reduced margin.....	34
Table 9 Hypothetical margin for DIR uncertainty .....	36

## List of Figures

Figure 1 General workflow of the radiation therapy .....	2
Figure 2 The image quality comparison of different imaging modalities. ....	3
Figure 3 Daily anatomical changes due to the breathing variations of a breath-hold patient. ....	5
Figure 4 Flow chart of the deformable image registration.....	12
Figure 5 Flow chart to evaluate the target coverage based on clinical practice .....	14
Figure 6 Flow chart to obtain the optimized margin .....	16
Figure 7 Flow chart to obtain the benefit margin to account for uncertainties in DIR .....	17
Figure 8 Merged images of the liver patient after DIR in the axial, sagittal and coronal views. ....	19
Figure 9 Merged images of the prostate patient after DIR in the axial, sagittal and coronal views. ....	20
Figure 10 Merged images of the breast patient after DIR in the axial, sagittal and coronal views. ....	21
Figure 11 Day to day variation of the axial, sagittal, and coronal views of the liver case L-4. ....	24
Figure 12 The axial volume deviation (same cut) of case L-8.....	24
Figure 13 The deformed tumor coverage of the axial, sagittal, and coronal views of case B-4.....	25
Figure 14 Comparison of the EVM and the optimized margin based on multi-modality images for the liver cases .....	26
Figure 15 Comparison of the EVM and the optimized margin based on multi-modality images for the prostate cases .....	27

Figure 16 Comparison of the EVM and the optimized margin based on multi-modality images for the breast cases.....	27
Figure 17 Dose distribution map of L-1.....	30
Figure 18 Dose distribution map of P-1.....	33
Figure 19 Dose distribution map of B-1.....	35

## **Acknowledgements**

First, I would like to express my sincere gratitude to my supervisor, Lei Ren, for his instructive advice and encouragement on my research and thesis writing. I am deeply grateful of his help in the completion of this thesis. I am grateful to Dr. Yawei Zhang and Dr. Wendy Harris, for their valuable explanations on the technical details of my project. I also would like to thank David Huang for his valuable comments on the thesis writing. Moreover, I would heartily thank all the staff and peers at Duke Radiation Oncology Department for their assistance on my research. Finally, I would not forget to thank my parents who have supported my study.

# **1. Introduction and Background**

## ***1.1 General workflow of radiation therapy***

Radiation therapy has been commonly used to treat localized cancer because of its abilities to control cell growth or kill cells [1]. As shown in Fig.1, the workflow of radiation therapy includes simulation, treatment planning, patient set up, and treatment delivery. In simulation, CT/MR scan of the tumor region is acquired to localize the tumor volume. In treatment planning, the physicist will use treatment planning software to customize the radiation beams to achieve certain dose distribution for individual patients. Typically, the goal of radiation therapy is to deliver sufficient dose to the target while sparing the normal tissue. Many impactful techniques have been introduced into radiation therapy during the last two decades to achieve this goal [2]. One of the advancement is to deliver precise radiation doses to a specific area using the intensity-modulated radiation therapy (IMRT) technique to treat complicated tumor volume [3]. This technique requires an adequate target delineation, appropriate dose prescription, and dose-volume constraints to optimize the radiation patterns and spatial dose distributions using inverse planning techniques [4]. IMRT makes the dose distribution conformal to the shape of the PTV while sparing the surrounding normal tissues at the same time. Besides IMRT, there are also other techniques, such as volumetric arc therapy (VMAT), 3D, and dynamic conformal arc, to achieve different dose conformality and delivery efficiency.

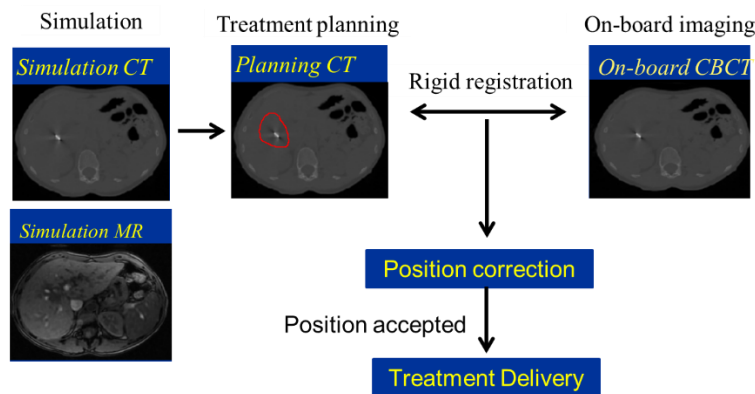


**Figure 1 General workflow of the radiation therapy**

In the patient set up, the therapist needs to check the patient position in the treatment room to ensure the on-board target position is in alignment with the planned target position. To achieve accurate delivery of the plan, the image-guided radiotherapy (IGRT) was introduced. IGRT uses various on-board imaging techniques to generate on-board 2D/3D images of the patient, which is then rigidly registered with the planning images to determine the shifts needed to align the patient with the planned position. In general, IGRT substantially improves the accuracy of the treatment delivery, which can potentially lead to better treatment outcome [5].

## 1.2 Challenges in soft tissue target localization

### 1.2.1 Limited soft tissue contrast in CBCT

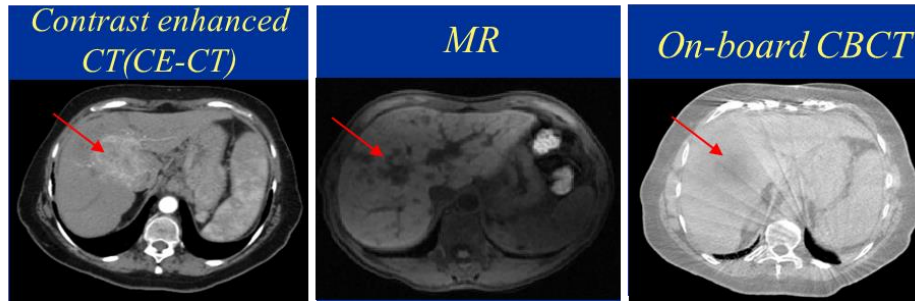


**Figure 2** The image quality comparison of different imaging modalities. The red arrow indicates the location of the tumor in the same cut.

Cone beam computed tomography (CBCT) is the most commonly used on-board 3D imaging technique to generate 3D/4D images of the patient for target localization in radiation therapy. To image large areas such as chest or abdominal regions, a half fan scan is typically used for CBCT acquisition, which scans over a full 360° rotation angle with the detector offset laterally by certain distance [6]. To image small areas such as brain region, a full fan scan is typically used which scans over around 200° with the detector centered to the central x-ray beam [7]. In recent study, the limited angle intrafraction verification (LIVE) was developed for four-dimensional target verification and 30° scan angle can accurately estimate the target volume [6].

However, CBCT has poorer image quality than the CT images in terms of image contrast and artifacts, partially due to the large amount of scatter caused by its large image view. As a result, the visualization of the target volume in the soft tissue, such as liver tumor, is rather limited in the CBCT [8]. This poor visualization of the target in

CBCT images would severely limit the accuracy of the target localization before each fraction of treatment [9]. As shown in Figure 2, because of the low soft tissue contrast and the streaking artifacts, the visualization of the tumor in the CBCT images is limited. In the contrast-enhanced CT(CE-CT) images and MR images, the tumor can be better visualized. CE-CT can find pathology by enhancing the contrast between a lesion and the normal surrounding structures and CE-CT with iodinated intravenous (IV) has been a gold standard to detect enhancement in a complex renal cyst [10]. MR images can usually provide good soft tissue contrast as well, and thus are useful for delineating the tumor target [11].

Because of the limited visualization of the tumor in CBCT, the rigid registration between the planning CT(P-CT) images and CBCT images is mainly based on the landmarks or the boundary of the organs with no direct verification of the target location inside the organ in clinical practice. This potentially leads to large errors in the localization and therefore requires larger PTV margins to account for the setup errors, which further limit our ability to escalate the PTV dose and spare the normal tissues.

### 1.2.2 Patient setup variations

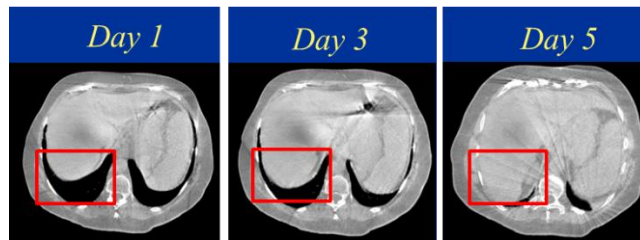


**Figure 3 Daily anatomical changes due to the breathing variations of a breath-hold patient. Images were taken in the same cut. The red box indicates the boundary of the liver.**

In conventional CBCT guided radiation therapy, the therapist manually registers the planning CT images with the CBCT images to verify the patient position based on the location of the target and normal tissues before the delivery of the beam. However, patient anatomy in CT and CBCT images can be quite different due to all sources of patient setup variations, which complicate the process of target localization.

The main difference in CT and CBCT images is the patient setup variations, which can be classified into three categories based on the causing factors: patient movement, inaccurate patient positioning, and organ motion due to physiological process such as breathing [12]. Typically, the patient movement and inaccurate patient positioning can be minimized by using the immobilization device and the image guidance. The organ motion due to physiological process can be classified into two categories based on the relevance with the treatment: gradient change caused by the treatment effects (weight loss or tumor regression), and the normal physiologic processes [13]. The normal physiologic organ motion can be divided into two categories

based on the repetition: peristaltic irregular deviation (such as organ motion and variations in bladder filling) and cyclical (predictable, respiratory movement) [13-15].

The physiological organ motion can also be classified into two categories based on the happening stage: interfraction organ motion and intrafraction organ motion [12]. The interfraction organ motion alters the day to day boundary and the inner anatomical structure distribution of soft tissue. These changes are not properly considered before the beam delivery, causing some uncertainties in the treatment [16]. The intrafraction organ motion set up error refers to the patient motion during treatment delivery. This type of motion is typically related to factors such as internal organ motion changes during the treatment fraction, decreasing the accuracy of radiation delivery [17, 18].

The organ motion due to physiological process is taken into account by the use of various margins during planning. The International Commission on Radiation Units and Measurements (ICRU) Report 50 and 62 recommends gross tumor volume(GTV), clinical target volume(CTV), internal target volume(ITV), and planning target volume(PTV) to be identified in a treatment plan. The GTV is defined as the demonstrated extent and location of the tumor [19]. The CTV is defined as the GTV plus a margin that represents the suspected tumor (clinical margin). The ITV is defined as the CTV plus a margin to account for the organ motion due to the physiological process (internal margin). The PTV is defined as the ITV plus a margin due to the uncertainties in patient positioning and patient movement (setup margin). The target volume is identical to the PTV based

on International Commission on Radiation Units and Measurements (ICRU) Report 29 [20].

However, for target volume with significant respiratory motion, the internal margin and setup margin would cause irradiation of a large volume of healthy tissue, increasing the risk of complications [21]. This will be especially of a concern for hypofractional stereotactic body radiotherapy [22, 23].

### ***1.3 Deformable image registration (DIR)***

#### **1.3.1 Image registration in radiation therapy**

In radiation therapy, the imaging datasets acquired have significantly increased after the introduction of the target delineation devices and the IGRT devices. Image registration is the process of transforming different sets of data into one reference coordinate system [24]. Images acquired by the same or different imaging modalities are used to determine the spatial transformation or combining information. In radiation therapy, image registration is broadly used in treatment planning and patient position verification. Image registration can be divided into two categories: 1. Rigid registration, which involves a single displacement vector, consisting of three orthogonal translations, and three angular rotations. The pixel-to-pixel spatial relationship remains the same before and after the registration [2]. Rigid registration has been broadly used in radiation therapy (e.g., CT-to-MR registration, CT-to-CBCT registration). It is widely recognized that rigid registration is very effective when no significant deformation of

anatomical structures is expected [2]. 2. Deformable image registration registers the deformation between two image sets by assigning a deformation vector field to each voxel [13]. Compared with rigid registration, the DIR has a greater number of degrees of freedom.

### **1.3.2 Brief introduction of deformable image registration (DIR)**

DIR was firstly developed in the 1980s for brain surgery and neuroscience [2].

The DIR applications in radiation therapy can be categorized into four major fields: dose accumulation, mathematical modeling, automatic segmentation and functional imaging.

Dose accumulation uses the displacement vector field (DVF) to map a dose distribution from the deformed image to a reference image. Mathematical modeling uses the transformation information to find the motion or deformation in certain organ.

Automatic segmentation deforms the contours in a reference image to CT images for segmentation during the treatment course. Functional imaging uses the deformable vector field to indicate the volume changes in images [13, 25].

The result of DIR is a deformation vector field which describes the correspondence between the voxels in the source and target images. DIR can be classified into two categories based on the objective function (matching criteria): intensity-based objective registration and feature-based registration. The first DIR category computes the similarity index between intensity values in the source and the target images, which can be used for single modality or multi-modality images. The

similarity index used in DIR are squared error (SE), correlation coefficient (CC), and mutual information (MI). SE is sensitive to noise in images and does not work well with multi-modality images. CC and MI are less sensitive to noise or image intensity differences between source and target images, and therefore can be used for multi-modality image registration [25]. The registration can be regarded as a process to maximize the similarity index between the source and the target images. The feature-based image registration include contour based and control point-based registration. The contour-based method registers the contours between the source and target images, while the control point-based method registers the corresponding control points. The deformation of other voxels is based on basis functions or biomechanical modeling. Feature based registration is suitable for multimodality image registration [2].

The transformation model (basis function) is used to save effort and reduce errors by automating the building and modification [26]. A deformable transformation model needs motion parameters to complete local transformation. The position of the point of interests (POIs) between images are updated based on the transformation model to maximize the similarity index [2]. The Velocity AI model used in our research based on the B-spline based model. It is a parametric model, which can automatically select the control points and determine the displacement of any nearby points by B-spline interpolation [27].

There are three methods commonly used to evaluate the DIR: (1) digital phantoms, (2) physical phantoms, and (3) real patient data based on the anatomical landmarks. In real patient data, it is challenging to evaluate the DIR results due to lack of ground truth. Evaluating the registration accuracy of anatomical landmarks is commonly used to evaluate the accuracy of DIR [2]. In our research, this method is also used to evaluate the result of DIR.

#### **1.4 Research aim**

Since MR or CT images can usually provide good soft tissue contrast and is often used for delineating the tumor target [11], the approach of using deformable image registration (DIR) to generate high resolution on-board multi-modality images would potentially improve the target localization accuracy.

This study evaluates the feasibility of using DIR to generate on-board multi-modality images to improve the target localization accuracy in radiation therapy. The research includes three aims: (1). Evaluate whether the registration and margin design in clinical practice is sufficient to ensure the coverage of the deformed tumor. (2). Evaluate the potential for margin optimization based on the synthetic multi-modality imaging technique. (3). Evaluate the effects of hypothetical DIR uncertainties on the optimized PTV margin. The development can potentially allow us to achieve more accurate target localization and optimize the PTV margin for individual patients.

## **2. Materials and Methods**

### ***2.1 Generation of on-board multi-modality images***

#### **2.1.1 Image acquisition**

MRI and CT images were acquired during the simulation stage for treatment planning. For the 8 liver SBRT patients, the MRI\_T1 FSPGR (Fast Spoiled Gradient Recalled Echo) or the contrast-enhanced CT (CE-CT) images are used as the prior images. The tumor contour on the MR/CT was delineated by the oncologist. Patients labeled as L-1, L-3, L-4, and L-7 were scanned with breath-hold to obtain the simulation images with CTV as the tumor contour. Patients labeled as L-2, L-5, L-6 were scanned with free breathing with ITV as the tumor contour. For the 7 prostate patients, the CT images are used as the prior images. For the 7 breast patients, the supine position was used for simulation and treatment to reduce the breath uncertainty. The CT images with CTV as the tumor contour were set as the prior images. Daily CBCT images were acquired on-board for each patient. These patient images sets were exported from Eclipse (Varian Medical Systems) and anonymized for the deformable image registration (DIR).

## 2.1.2 Deformable image registration

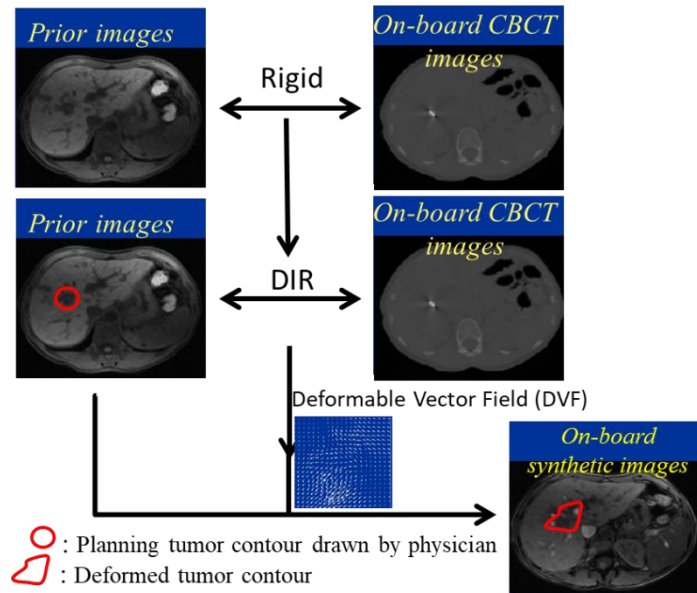


**Figure 4** Flow chart of the deformable image registration

The anonymized images were imported to the Velocity AI (Varian Medical Systems) software for image registration. The MR/CT images were set as the source images and registered with the CBCT images to generate synthetic on-board images according to the Velocity AI manual. In brief, this registration includes two parts: (1) A rigid registration between the images to translate and rotate the two images closer before starting a deformable registration. (2) A B-spline algorithm based deformable registration. The CBCT/MR corrected single pass deformable registration tools were applied for this process in Velocity AI. Then the result of DIR is quantified as deformable vector field (DVF), which indicates the flow of each pixels [28]. Then the DVF was used to propagate the tumor contour drawn by the physician to the synthetic

image coordinate to generate on-board tumor volume. For the liver, prostate, and breast, the region of interest (ROI) used in the registration were the whole images, the prostate and surrounding organs, and the breast with lesion, respectively.

### **2.1.3 Assessing the quality of DIR**

The most intuitive approach to validate the DIR algorithm is checking the anatomical landmarks on the merged images [2]. To determine a better modality of prior image for deformable image registration, the MR and CT images of the same patient were registered to the CBCT images. The quality of the DIR was checked in the merged images based on the alignment of the landmarks, such as the boundary of the target organ and the surrounding organs. For the prostate patients, the quality of deformable registration is checked via the shape of the bladder and rectum. To minimize the observer bias, the DIR quality was checked by two researchers independently. After comparison of the two scenarios of using different modality prior images, a better modality was selected and used for other cases. Then the images and contours were exported from Velocity AI for further on-board target localization and evaluation.

## ***2.2 Evaluation of the feasibility of the DIR based target localization***

The images and contours needed in this part are imported into Eclipse for further analysis. The evaluation includes three parts: (1). Evaluate whether the on-board rigid registration and the clinical margin design is sufficient to cover of the target volume: the synthetic on-board images are used to verify the target coverage based on the shifts

determined by the on-board registration in clinical practice; (2). Evaluate the potential for margin optimization based on the synthetic multi-modality imaging technique: shifts are determined by rigid registration between planning CT and synthetic on-board CT, and the optimized PTV margin is determined to ensure coverage of the deformed tumor volume. (3). Evaluate the effects of hypothetical DIR uncertainties on the margin optimization: shifts are determined by rigid registration between planning CT and the synthetic on-board MR/CT, and the tolerant margin is determined to cover the expanded deformed tumor volume without increasing the original PTV.

### 2.2.1 Evaluation of the deformed CTV coverage in clinical practice

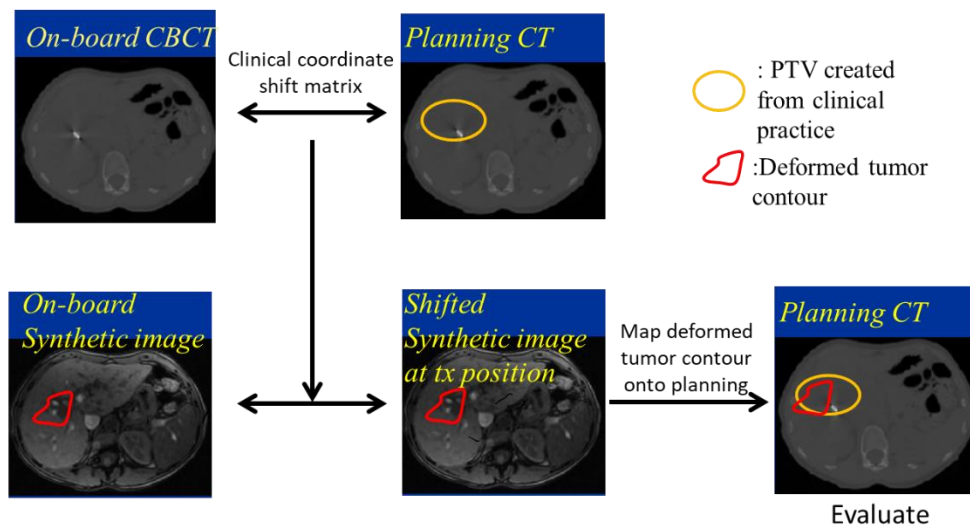


**Figure 5 Flow chart to evaluate the target coverage based on clinical practice**

The images and contours were imported into Eclipse patient data sets for evaluation. To evaluate the deformed CTV coverage in the clinical practice, the synthetic on-board images were used to verify the target coverage based on the shifts determined

by the on-board registration in clinical practice. The on-board shift matrix is a translational shift matrix reflecting the clinical rigid registration between the on-board CBCT images and the planning CT images. This matrix was used to translate the on-board synthetic images to the actual treatment position. The CTV volume in the shifted on-board synthetic images is then mapped onto the planning CT images to evaluate its coverage in the original clinical plan.

## **2.2.2 Evaluation of the potential to optimize the PTV margin and dosimetric effect**

### **2.2.2.1 Equivalent volume margin(EVM)**

In clinical practice, the tumor volume may be expanded anisotropically to protect some critical organs. To simplify the representation of the original planned margin, the concept of Equivalent Volume Margin(EVM) was used to quantify the original planned margins. EVM is defined as the isotropic margin that would result in the same PTV volume as the planned PTV with anisotropic margins.

### 2.2.2.2 Optimization of the CTV/ITV to PTV margin

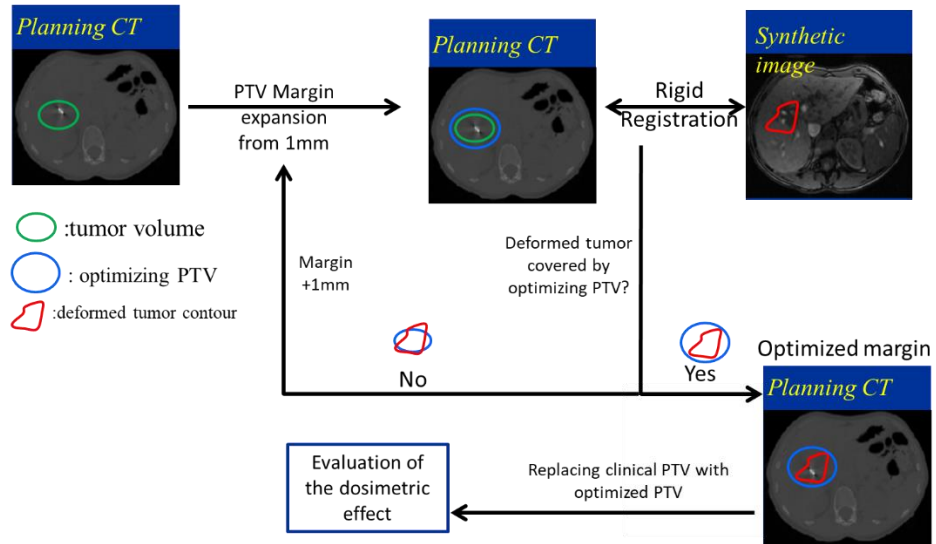


**Figure 6 Flow chart to obtain the optimized margin**

A minimum optimized ITV to PTV margin will be determined to ensure the target coverage based on the synthetic on-board images. To obtain the minimum margin, the tumor volume on the planning CT was first expanded by 1mm to generate a PTV. The planning CT images was translationally shifted to register with the synthetic image to verify if the PTV is able to cover the tumor volume in the synthetic on-board images. The tumor coverage was checked slice by slice on three sectional views. If the generated PTV is not large enough to cover the deformed tumor volume in the synthetic images, the PTV margin would be expanded further until it was sufficient to cover the on-board tumor volume. The final margin determined is regarded as the optimized PTV for the dosimetric evaluation. The optimized margin was also compared with the EVM to determine the reduction or increment of the CTV/ITV to PTV margin.

### 2.2.2.3 Evaluation of the dosimetric effects

The dosimetric effect of using the optimized PTV was evaluated in Eclipse. The clinical PTV was replaced by the optimized PTV. The constraints and other settings of the optimized plan are controlled the same as the clinical plan. The optimization of the dose distribution was continued with the clinical fluence. Then the volume dose was recalculated. The clinical plan and optimized plan were compared using the computed DVH and isodose wash map. The dose to the organ at risk(OAR) was also compared based on the constraints.

### 2.2.3 Evaluation of the hypothetical margin to account for uncertainties in DIR

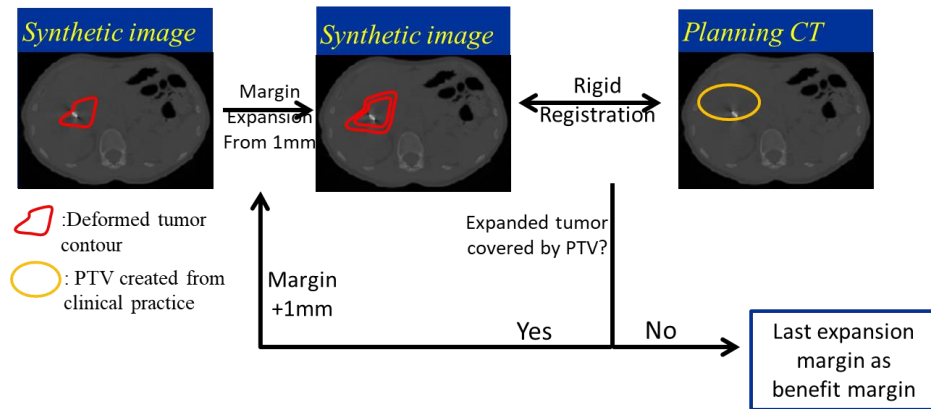


**Figure 7 Flow chart to obtain the benefit margin to account for uncertainties in DIR**

Since the deformable registration uncertainty was difficult to estimate directly, the hypothetical margin for this uncertainty based on the deformed tumor contour was used to quantify the potential tolerance for this uncertainty in our research. The deformed tumor contour was first expanded by 1mm in the synthetic images. Then the synthetic

images were registered to the planning CT using a translational shift. The expanded contour coverage in the original is checked slice by slice on three sectional views. If the PTV is large enough to cover the expanded volume, the expanded volume will expand by another 1mm. Otherwise this process will stop, and the last margin is regarded as the benefit margin.

### 3. Results

#### 3.1 DIR quality comparison of using CT/MR as the prior images

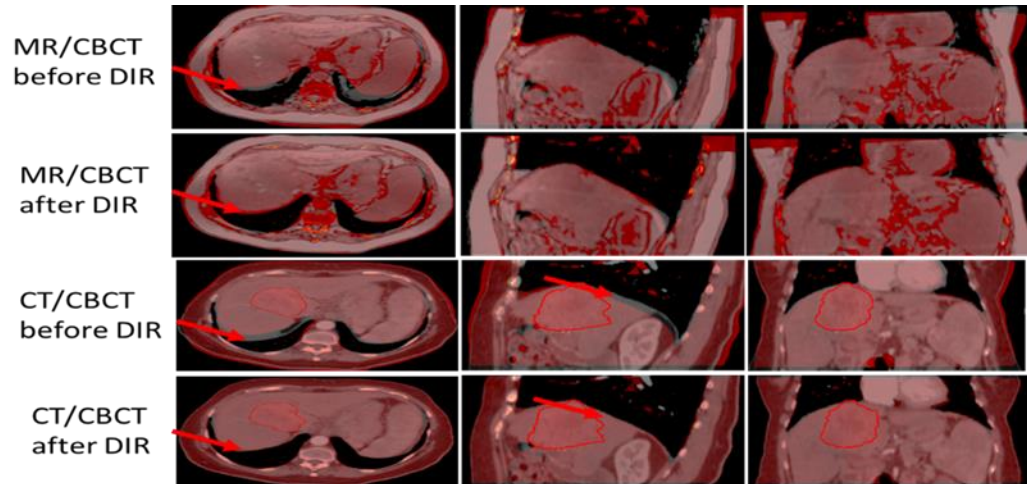
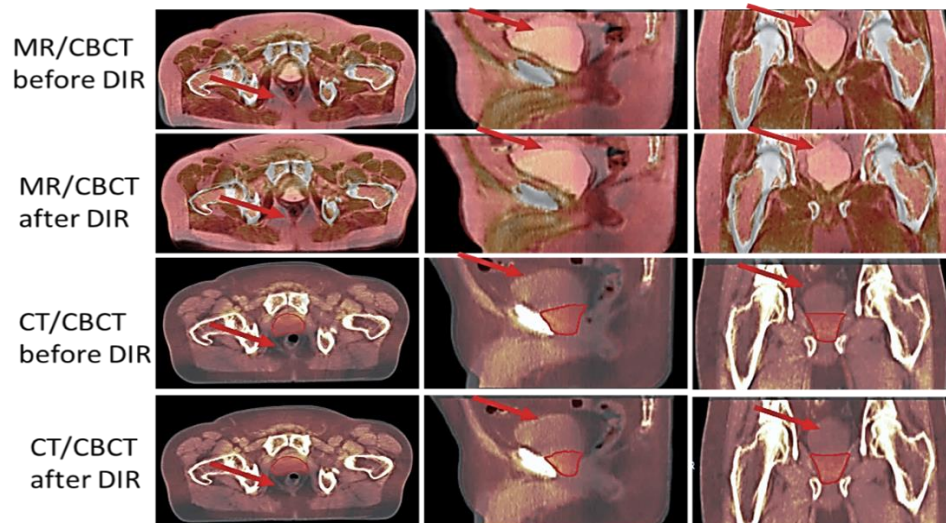


Figure 8 Merged images of the liver patient after DIR in the axial, sagittal and coronal views. The prior images and CBCT images are red and gray respectively. The CBCT images are the same cut of the same patient. The red arrow indicates the boundary of the liver. The contrast enhanced CT(CE-CT) images use breath-hold modality. The red contour indicates the tumor contour before DIR and deformed tumor contour after DIR.

For the liver cases, before DIR the boundary of the liver does not match in the axial view of the MR/CBCT merged images and the CE-CT/CBCT merged images. In the sagittal view of the merged CE-CT/CBCT images, the altitude of the diaphragm on CBCT images was higher than on the CT images. After DIR, the MR liver boundary extended out of the CBCT liver boundary (Fig. 8, red arrow in second line) while the CT

liver boundary aligns well with the CBCT liver boundary (Fig. 5, fourth line, red arrow).



**Figure 9 Merged images of the prostate patient after DIR in the axial, sagittal and coronal views. The prior images and CBCT images are red and gray respectively. The CBCT images are the same cut for the same patient. The red arrow indicates the boundary of the rectum and bladder. The red contour indicates the tumor contour before DIR and deformed tumor contour after DIR.**

For the prostate cases, the main landmarks used to control the quality of the DIR are the bladder, and the rectum. The alignment of the boundary of the landmarks on the MR to CBCT merged does not change significantly after DIR. The bladder level is quite different in the MR/CBCT merged images while the alignment in the CT/CBCT merged images is better. However, the rectum boundary does not align well with the CBCT images for both modalities.

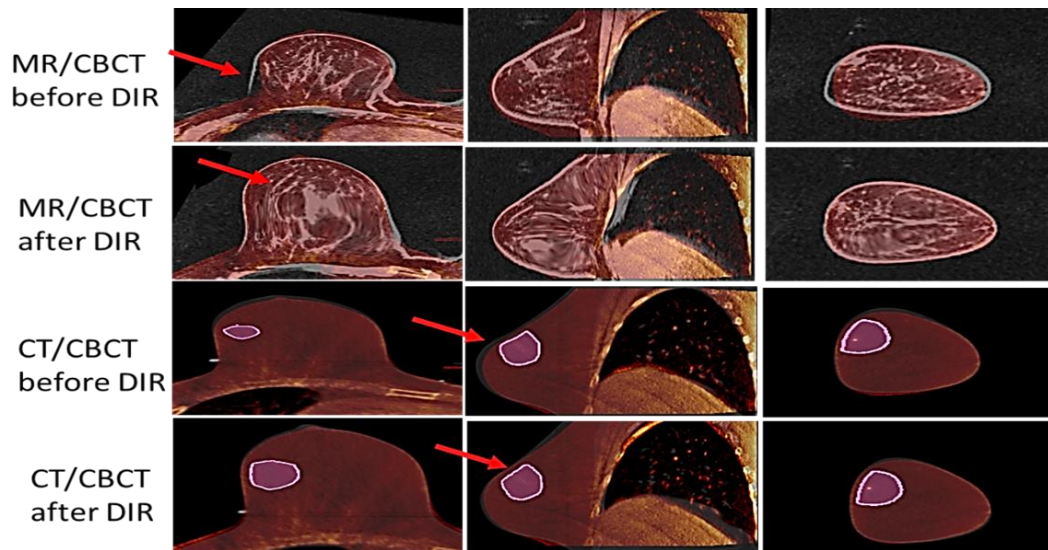


**Figure 10 Merged images of the breast patient after DIR in the axial, sagittal and coronal views. The prior images and CBCT images are red and gray respectively. The CBCT images are the same cut for the same patient. The red arrow indicates the boundary of the breast. The red contour indicates the tumor contour before DIR and deformed tumor contour after DIR.**

For the breast cases, after DIR the breast boundary matched well for the two-modalities. However, the MR/CBCT merged images shows unrealistically deformed ducts inside of the breast after DIR. The changes in the breast is large and the internal anatomical structures were strongly distorted on the deformed MR images, which strongly influences the location of the tumor and makes this modality unreasonable for target localization. As compared with this, the change of internal anatomical structures in CT to CBCT DIR is less.

### 3.2. Results of the coverage of the CTV based on clinical shifts

Table 1 Coverage of the deformed tumor volume based on clinical shifts for liver patients

Treatment day	Patient #							
	L-1	L-2	L-3	L-4	L-5	L-6	L-7	L-8
Plan	100	100	99.2	99.7	100	100	100	100
Day 1	97.6	100	100	99.9	94.2	100	100	86.6
Day 2	98.5	100	99.1	99.1	96.3	100	100	76
Day 3	99.6	100	94.4	99.9	98.1	100	100	100
Day 4	99.4		99.3	98.6	96.4	100	100	
Day 5	99.8		97.8	96.7	90.6	100	100	
Day 6				94.5				
Day 7				93.6				
Day 8				90.2				
Day 9				90.7				
Day 10				88.2				

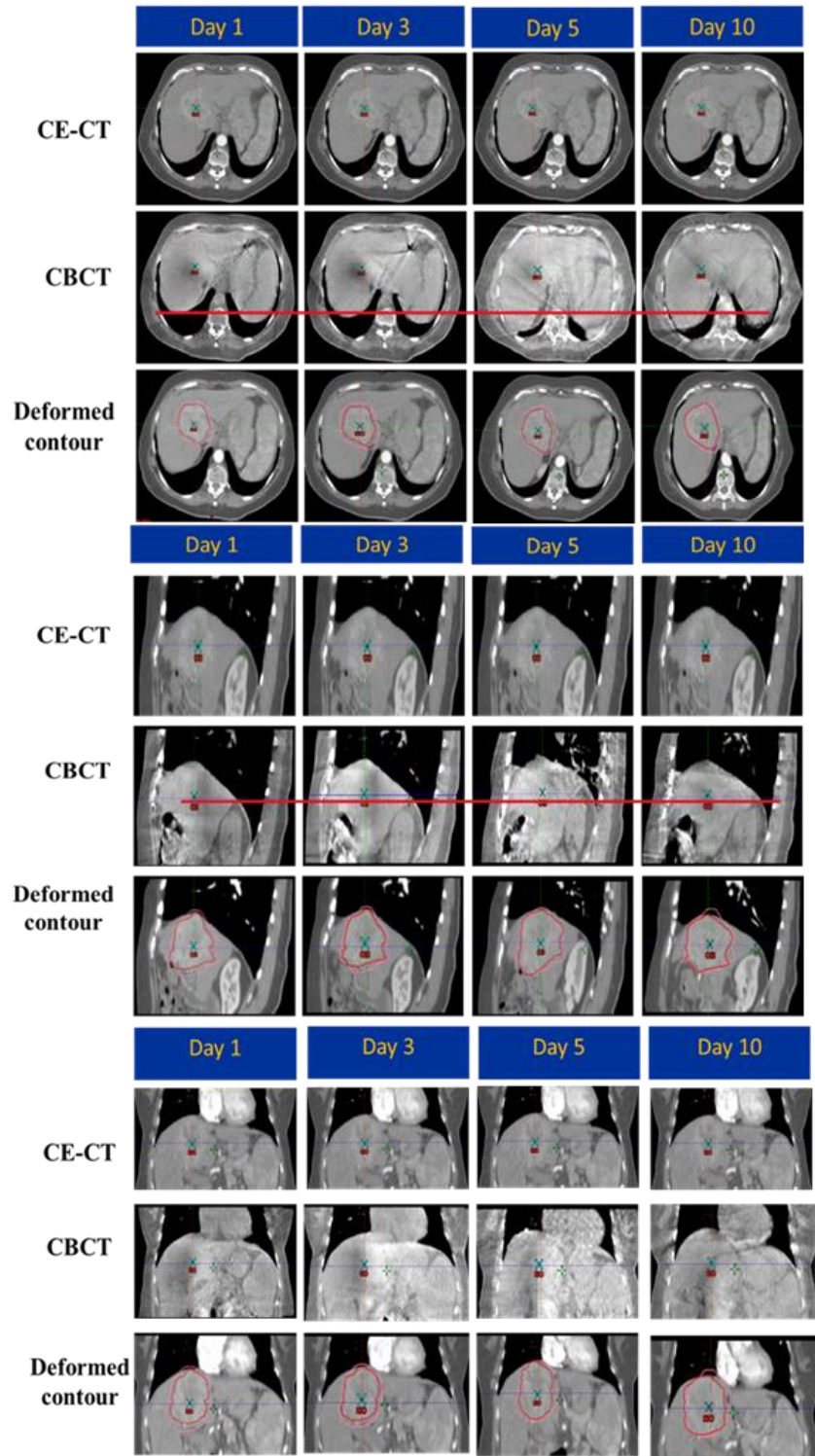


Figure 11 Day to day variation of the axial, sagittal, and coronal views of the liver case L-4. The pink contour indicates the PTV; the red contour indicates the deformed tumor contour. The line is reference to indicate the location of the liver and lung.

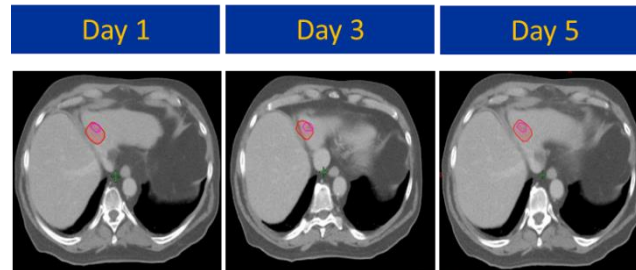


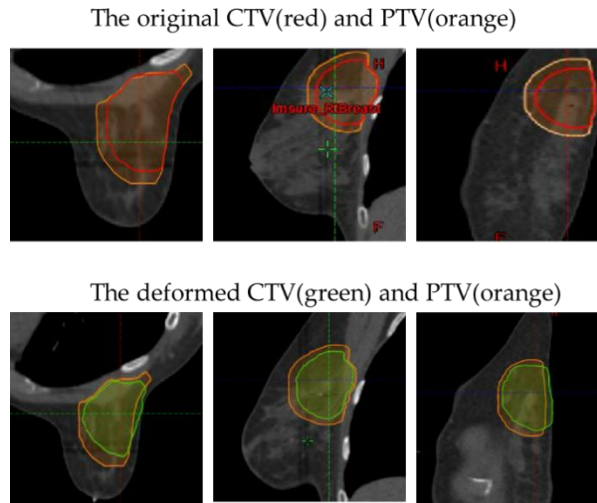
Figure 12 The axial volume deviation (same cut) of case L-8. The red contour indicates the PTV; the crimson contour indicates the deformed tumor contour.

Table 2 Coverage of the deformed tumor volume based on clinical shifts for prostate patients

	Treatment day	Patient #						
		P-1	P-2	P-3	P-4	P-5	P-6	P-7
	Plan	100	100	100	99.98	99.97	100	100
Tumor volume coverage (%)	Day 1	100	96.02	100	94.62	100	100	96.45
	Day 5	100	100		99.96		100	
	Day 10		100		96.89			
	Day 15				100			
	Day 20				100			
	Day 25				100			
	Day 28				100			

Table 3 Coverage of the deformed tumor volume based on clinical shifts for breast patients

	Treatment day	Patient #						
		B-1	B-2	B-3	B-4	B-5	B-6	B-7
Tumor volume coverage (%)	Plan	98.69	97.55	99.65	95.5	97	100	96.48
	Day 1	99.8	97.78	98.76	87.9	93.36	97.1	90.21



**Figure 13 The deformed tumor coverage of the axial, sagittal, and coronal views of case B-4. The green contour indicates the deformed tumor contour; the orange contour indicates the PTV.**

For the liver cases, the deformed CTV coverage of 6 cases (8 cases in total) is above 90%. The lowest coverage is 76% in the case of L-8 (Tab. 1). For the prostate cases, the coverage of all the cases is above 94% (Tab. 2). For the breast cases, the coverage is above 90% except patient B-4, and case B-4 has the lowest coverage of 87.9% (Tab. 3). The average coverage for liver, prostate, and breast are 97.4%, 99.3%, and 96.4% respectively.

The cases with coverage less than 90% were rechecked with the PTV, deformed tumor contour, and the patient images. For case L-4, generally the coverage decreases as treatment days increase. The CBCT images (Fig. 11) shows the volume of the lung and the altitude of the liver were changing during the treatment course, which led to large localization errors. For patient L-8, the deformed CTV coverage has a larger deviation.

As shown in CBCT images figure 12, the PTV volume (14.9 cc) of this case is relatively small as compared with the PTV of other liver patients (45-414 cc), suggesting there might be a large percentage deviation when deformed. For case B-4, there is no margin between the CTV and the PTV on some direction of the target to protect the critical organs. As a result, part of the GTV got out the PTV after DIR (Fig. 13). For these 3 cases, the margin design and CBCT-CT rigid registration may not be sufficient for target coverage.

### **3.3 Evaluation of the potential to optimize the PTV margin and dosimetric effect**

#### **3.3.1 Equivalent volume margin(EVM) and multi-modality margin**

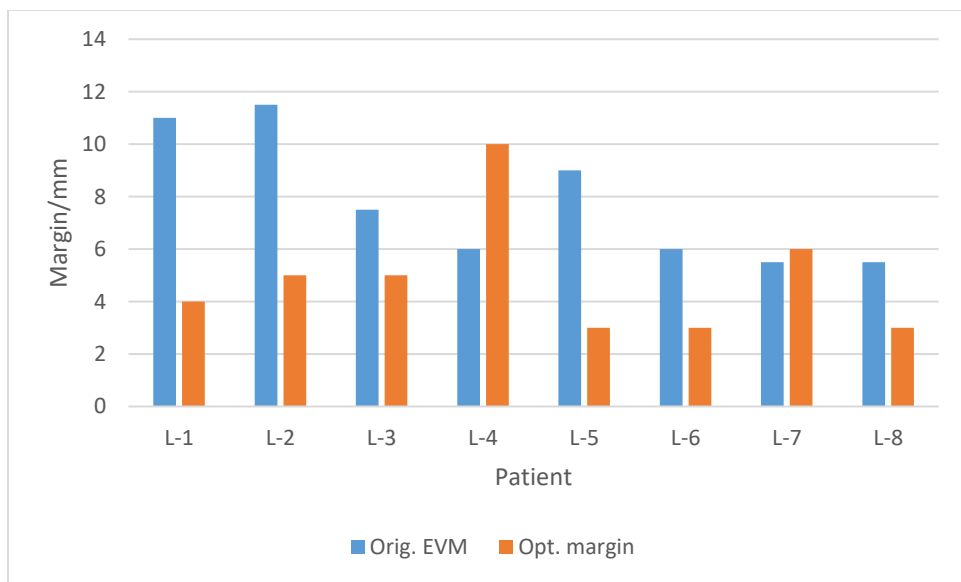


**Figure 14 Comparison of the EVM and the optimized margin based on multi-modality images for the liver cases**

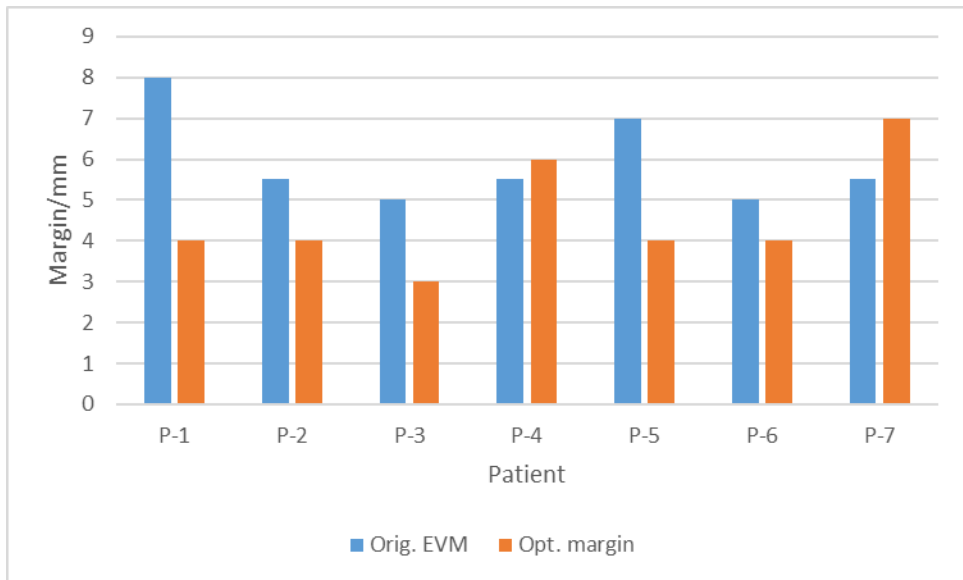


**Figure 15 Comparison of the EVM and the optimized margin based on multi-modality images for the prostate cases**

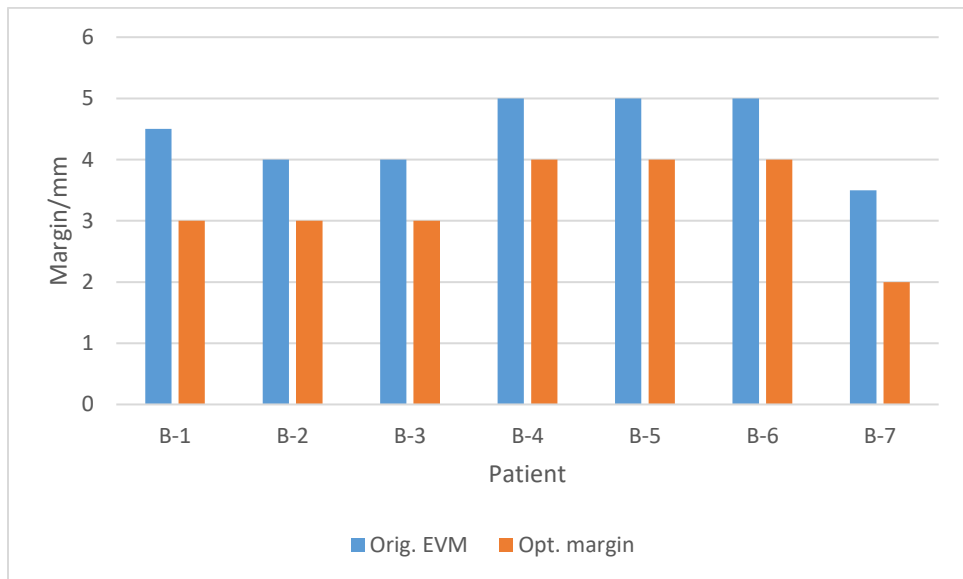


**Figure 16 Comparison of the EVM and the optimized margin based on multi-modality images for the breast cases**

For most of the liver, prostate, and breast cases, the synthetic images allowed the reduction of PTV margin, which is up to 6mm, 4mm, and 1.5 mm, respectively. For

patient L-4, L-7, P-4, and P-7, the margin needed was increased by 4mm, 0.5mm, 0.5mm, and 1.5 mm respectively (Fig. 14, 15, and 16).

### **3.3.2 Dosimetric evaluation**

#### **3.3.2.1 Dosimetric evaluation of the liver SBRT cases**

**Table 4 Dosimetric comparison of the original plan and optimized plan for liver cases with reduced margin**

Pt #		Liver /cc	Cord D <sub>max</sub> /Gy	Bowel D <sub>max</sub> /Gy	Stomach D <sub>max</sub> /Gy	Chest wall V>30Gy	Right Kidney D <sub>max</sub>	Esophagus D <sub>max</sub>	Heart D <sub>max</sub>	Skin D <sub>max</sub>	Hilum <25 Gy	Duodenum D <sub>max</sub>	Left Kidney >18Gy
L-1	Orig.	<12Gy 868	11.69	0.95	15.61	24.1cc		21.37	29.5				
	Opt.	<12Gy 894	12.48	0.95	15.72	14cc		17.67	27.64				
L-2	Orig.	<15Gy 906.7		9.76	14.82	37.7cc	<10Gy 48%			26.88	91.3%		
	Opt.	<15Gy 933.5		8.3	11.8	17.4cc	<10Gy 52.1%			21.4	92.8%		
L-3	Orig.	< 12Gy 1945.95		7.67	1.74	11.64cc	8.8			17.98		0.19	
	Opt.	< 12Gy 1975.42		5.58	1.63	7.85cc	7.86			16.7		0.16	
L-5	Orig.	<20Gy 1036.1	17.2	4.4					5				0
	Opt.	<20Gy 1075.5	14.52	4.29					2.02				0
L-6	Orig.	<20Gy 2463.9	7.2				23.8	0					
	Opt.	<20Gy 2529.1	6.8				21.9	0					
L-8	Orig.	<15Gy 1528.9			>30Gy 0		0.4	>30Gy 0	>30Gy 0				
	Opt.	<15Gy 1534.9			>30Gy 0		0.4	>30Gy 0	>30Gy 0				

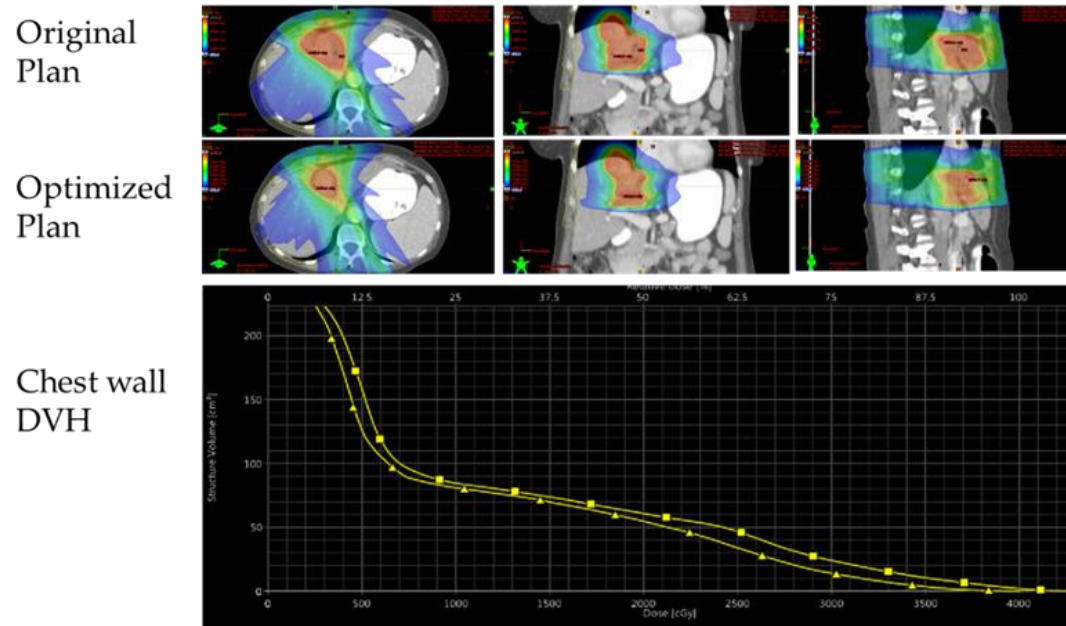


Figure 17 Dose distribution map of L-1. In the DVH, the square line and the triangle line indicates the original plan and the optimized plan, respectively.

Table 5 Dosimetric comparison of the original plan and optimized plan for liver cases with increased margin

Pt #		Margin /cm	Liver/cc	Cord D <sub>max</sub> /Gy	Bowel D <sub>max</sub> /Gy	Stomach D <sub>max</sub> /Gy	Chest wall	Heart
L-4	Orig.	6	< 15Gy 648.6	23.3	>40Gy 1.55cc	0		
	Opt.	10	< 15Gy 586.0	26.9	>40Gy 9.67cc	0		
L-7	Orig.	5.5	<15Gy 1411.8	8.4		>20Gy 0	>20Gy 0	>40Gy 0
	Opt.	6	<15Gy 1411.7	9.1		>20Gy 0	>20Gy 0	>40Gy 0

For liver SBRT cases with optimized plan, more of the normal tissue is spared with the same constraints. For patients L-1 and L-2, the dose to the chest wall decreased significantly with the optimized margin. For case L-1, the normal liver volume less than 12 Gy increased by 26 cc (Tab.7). The chest wall volume larger than 30 Gy decreased by 10 cc (41%). The wash map of case L-1 shows the red area (high dose) decreased and optimized dose volume histogram of the chest wall is lower than the original one. For liver SBRT cases with equal or increased margin, the dose to the OARs does not changed significantly due to the increased margin in the optimized plan.

### 3.3.2.2 Dosimetric evaluation of the prostate cases

**Table 6 Dosimetric comparisons of the original plan and new plan for the prostate cases with reduced margin**

Pt#		Bladder V>70Gy	Bladder V>65Gy	Bladder V>40Gy	Rectum V>70Gy	Rectum V>65Gy	Rectum V>40Gy	Left Femoral head V>50Gy	Right Femoral head V>50Gy	Penile bulb
P-1	Orig.	0	14.6%	19.9%	0	0.9%	6.7%	0	0	>30Gy 100%
	Opt.	0	11.7%	18.0%	0	0.4%	5.8%	0	0	>30Gy 100%
P-2	Orig.	10.8cc	3.2%	7.4%	1.9cc	3.5%	11.5%	0	0	mean 3.6Gy
	Opt.	9.1cc	2.9%	7.0%	0.8cc	2.8%	11.1%	0	0	mean 3.5Gy
P-3	Orig.	4.0cc	3.2%	14.1%	2.0cc	2.3%	12.1%	0	0	mean 6.1Gy
	Opt.	1.5cc	2.0%	12.5%	0.7cc	1.4%	10.9%	0	0	mean 5.9Gy
P-5	Orig.	0	24.2%	40.0%	0	7.0%	31.5%	0	0	>30Gy 99.9%
	Opt.	0	24.2%	40.0%	0	6.5%	31.2%	0	0	>30Gy 99.9%
P-6	Orig.	D <sub>max</sub> =39.4Gy	> 24 Gy= 15.7 cc		≤ 33 Gy 89.1%	≤ 28 Gy 81.7%		≤ 24 Gy 75.8%	D <sub>max</sub> 14.8Gy	D <sub>max</sub> 16.7Gy
	Opt.	D <sub>max</sub> =39.7Gy	12.8 cc		89.8%	82.6%		≤ 24 Gy 76.8%	D <sub>max</sub> 14.4Gy	D <sub>max</sub> 16.5Gy

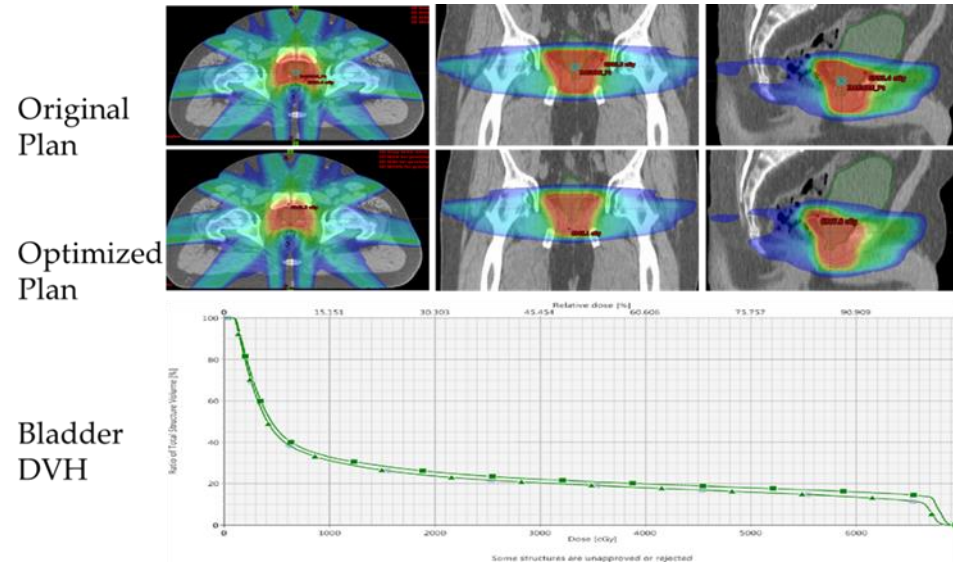


Figure 18 Dose distribution map of P-1. In the DVH, the square line and the triangle line indicates the original plan and the optimized plan, respectively.

Table 7 Dosimetric comparison of the original plan and optimized plan for prostate patients with increased margin

Pt#		Margin /mm	Bladder V>70Gy	Bladder V>65Gy	Bladder V>40Gy	Rectum V>70Gy	Rectum V>65Gy	Rectum V>40Gy	Light Femoral head V>50Gy	Right Femoral head V>50Gy	Penile bulb
P-4	Orig.	5.5	1.0cc	0.8%	3.5%	0.1cc	1.9%	12.0%	0	0	mean15.9Gy
	Opt.	6	1.4cc	1.0%	3.8%	1.1cc	4.0%	13.2%	0	0	mean13.6Gy
P-7	Orig.	5.5	0	32.61%	52.54	0	7.39%	46.29%	0	0	>30Gy76.29
	Opt.	7	0	32.95%	49.94	0	10.38%	40.86%	0	0	>30Gy71.95

### 3.3.2.3 Dosimetric evaluation of the breast case

**Table 8 Dosimetric comparison of the original plan and optimized plan for the breast cases with reduced margin**

Pt#		Normal breast V50%	Normal breast V100%	Contra-lateral breast V10%	Lungs mean /Gy	Lungs V8/GY	Lungs V7GY	heart MEAN /Gy	Heart D <sub>MAX</sub> /Gy	CW D20CC /Gy	Skin <sub>MAX</sub> /Gy	Skin V12GY	Cord <sub>MAX</sub> /Gy
B-1	Orig.	22.74%	5.61%	0%	0.24/0.38	0	0	0.43	3.38Gy	7.93Gy	18.83Gy	5.15%	0.05Gy
	Opt.	21.97%	4.48%	0%	0.24/0.34	0	0	0.36	2.95Gy	7.57Gy	18.85Gy	4.86%	0.05Gy
B-2	Orig.	28.69%	10.37%	0%	0.05/1.39	0%/0.58%	0%/1.35%	0.12	3.24Gy	8.35Gy	20.33Gy	5.25%	2.09Gy
	Opt.	25.39%	8.32%	0%	0.05/1.35	0%/0.67%	0%/1.25%	0.11	3.27Gy	7.87Gy	21.14Gy	4.95%	2.22Gy
B-3	Orig.	26.57%	10.07%	0%	0.01/0.99	0%/0.10%	0%/0.26%	0.08	2.29Gy	6.8Gy	19.71Gy	3.09%	0.52Gy
	Opt.	25.27%	8.95%	0%	0.01/0.99	0%/0.09%	0%/0.28%	0.07	2.28Gy	6.6Gy	19.02Gy	2.74%	0.50Gy
B-4	Orig.	29.92%	11.34%	0%	0.01/1.03	0%/0.33%	0%/0.56%	0.04	2.16Gy	9.38Gy	20.36Gy	3.43%	0.34Gy
	Opt.	27.88%	10.23%	0%	0.01/1.14	0%/0.56%	0%/0.95%	0.04	1.86Gy	9.35Gy	19.89Gy	3.04%	0.26Gy
B-5	Orig.	19.49%	4.50%	0%	0.39/0.06	0	0	0.3	2.3Gy	4.75Gy	18.87Gy	3.95%	1.07Gy
	Opt.	19.32%	4.02%	0%	0.42/0.06	0	0	0.29	2.34Gy	5.01Gy	18.77Gy	3.56%	1.2Gy
B-6	Orig.	13.6%	4.06%	0%	0.01/0.4	0	0	0.02	0.26Gy	1.93Gy	18.03Gy	2.8%	0.04Gy
	Opt.	13.38%	3.68%	0%	0.01/0.39	0	0	0.02	0.25Gy	1.90Gy	17.8Gy	2.64%	0.04Gy
B-7	Orig.	15.95%	4.6%	0%	0.01/0.59	0	0	0.03	0.7Gy	2.21Gy	19.11Gy	3.75%	0.06Gy
	Opt.	12.84%	3.299%	0%	0.01/0.44	0	0	0.02	0.33Gy	1.68Gy	19.14Gy	3.08%	0.05Gy

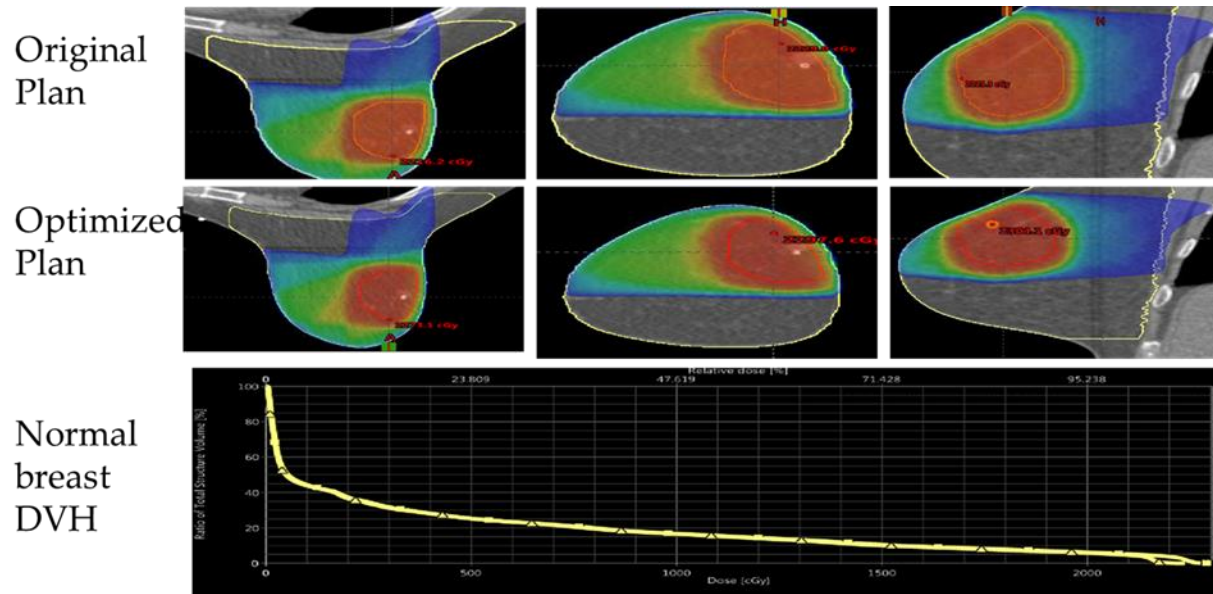


Figure 19 Dose distribution map of B-1. In the DVH, the square line and the triangle line indicate the original plan and the optimized plan, respectively.

For the prostate cases, 5 cases have reduced margin while 2 cases have increased margin. For case P-1, the bladder volume received larger than 65 Gy decreased by 3%. This is consistent with the wash map and the DVH curve. For the 2 cases with the increased margin, the rectum volume received more than 65Gy increased by 2-3% while other changes to the organ at risk are not significant. For the breast cases with a decreased margin, the spared dose is mainly on the normal breast. In the wash map, the high dose area shrinks but this is not significant on the normal breast tissue DVH. For cases with reduced margin, the optimized plan can spare more normal tissue. For the cases with equal or increased margin, the increased dose to the OARs does not change significantly.

### **3.4 Results of the evaluation of the hypothetical DIR uncertainty margin**

**Table 9 Hypothetical margin for DIR uncertainty**

liver cases	Patient #	L-1	L-2	L-3	L-4	L-5	L-6	L-7	L-8
	Hypothetical DIR Margin/mm	3	3	4	/	4	3	/	3
prostate cases	Patient#	P-1	P-2	P-3	P-4	P-5	P-6	P-7	
	Hypothetical DIR Margin/mm	4	1	3	/	5	1	/	
breast cases	Patient#	B-1	B-2	B-3	B-4	B-5	B-6	B-7	
	Hypothetical DIR Margin/mm	2	2	2	2	2	2	3	

For the liver cases, 7 patients have hypothetical margins in 2-4 mm. For the prostate cases, the hypothetical margin can be up to 5mm, but two cases have 1mm

margin and two cases have no hypothetical margin. For the breast cases, the hypothetical margin is 2-3 mm.

## **4. Discussion**

### ***4.1 Comparison of the MRI-based and CT images based deformable image registration***

The boundary-based DIR quality comparison of using MR/CT as the prior images shows using CT as prior images can achieve better alignment for liver, breast, and prostate cases, which is in coordinate with the report that MR to CT DIR has larger average absolute error than CT to CT DIR [29]. This indicates the algorithm force in the MRI boundary is not strong enough to match the CBCT boundary of the organs. The reason might be the different imaging principles of the CT and MR, which define different organ boundaries. Otherwise, for some cases, more visualized tissues in MRI also influence the movement of the pixels. An example is the breast MR to CBCT DIR: since the ducts with high intensity are invisible on the CBCT images while visible on MRI, the DIR algorithm forced to equal the inner gray intensity of the MRI, causing an over expansion of the tumor volume. For the prostate cases, the difference filling condition of rectum and bladder between the simulation and treatment strongly influenced the DIR result, causing the unsatisfying alignment of the boundary for both the MR to CBCT and CT to CBCT DIR. Even though using CT as prior images showed a better alignment, a relative large deformable uncertainty is still included. A better empty condition of the rectum and bladder is strongly suggested to achieve a better treatment accuracy.

## **4.2 Evaluation of the coverage based on the clinical practice**

In this research, for most cases, the tumor volume defined by the on-board synthetic images was mostly covered by the PTV based on the shifts applied in clinical practice. However, the clinical target localization using the current clinical margin may cause an over estimation of the tumor tissue. For liver, prostate, and breast, the CTV to PTV EVM in our study are 5.5-11.5mm, 5-8mm, and 3.5-5 mm respectively. Moreover, even though the rigid image registration is widely recognized an effective method when no anatomic change is expected [2], the interfraction organ motion changes the target location in soft tissue. As a result, the clinical shifts determined by the technician may have a large shift uncertainty. To ensure the coverage of the tumor volume, this uncertainty is taken into account when developing the PTV margin, which also causing over irradiation of the normal tissue.

Patient L-4 using breath-hold has the longest treatment days (10 fractions) and a relative small coverage (88.2%) among the 9 patients, suggesting the importance to account for the day to day patient deformation in margin design and on-board image registration. With the treatment days increasing, the breath-hole uncertainty increases, causing the tumor volume deformed more (Fig. 11). As a result, the planning target volume cannot cover the deformed tumor volume. The liver case L-8 has the lowest coverage in the liver cases. This can be explained by the relatively small PTV volume (14.9 cc), which makes the deformed part relative larger and generates a larger deviation

(S.D.=11.6mm while others are 0-4.4mm) when deformation happened. This case suggests the critical importance of accounting for the deformation when treating small tumors.

The average dose coverage for liver, prostate, and breast are 97.4%, 99.3%, and 96.4% respectively. The prostate cases have the largest coverage because the prostate is relatively far from the lung and less influenced by the breath as compared with the liver and breast. The breast treatment with the supine position has relatively small influence from the breath motion as compared with the liver [30]. This suggests the location of the organ also potentially influences the dose coverage of the deformed tumor volume because of the breath motion.

### ***4.3 The optimization of the margin and the dosimetric effect***

For most of the liver and prostate cases, the synthetic images allowed the reduction of the PTV margin by up to 6 mm and 4 mm, respectively. For the breast cases, the PTV margin is decreased by 1-1.5 mm, suggesting the breast with supine position is stable, and PTV margin can be reduced by 1 mm in clinical practice. This suggests that for most soft tissue cases, the synthetic images allowed the reduction of clinical margin. For patient L-4, L-7, P-4, and P-7, the margin needed was increased by 4 mm, 0.5 mm, 0.5 mm, and 1.5 mm respectively. The original margin designs are not sufficient for target coverage. Even though the optimized margin for the four cases are larger than the original margin, it does not mean the DIR based optimized plan is worse than the

original plan because the deformed tumor contour can provide more information about the target location and the optimized plan could potentially ensure the coverage of the target volume.

By using the optimized PTV with reduced margin for dose optimization, the dose can be spared to OAR based on the clinical constraints in practice. For the case L-1 using the optimized margin plan, the volume larger than 30 Gy decreased by up to 20 cc. The wash map shows the red area (high dose) decreased and the chest wall optimized dose volume histogram is lower than the original one. The spared OAR dose is significant for some specific tissues. Generally, the most commonly spared organ is the normal tissue volume. The maximum dose of the OAR does not change much according to the optimized plan. For the case with equal or increased margin, the maximum dose to the spinal cord and high dose volume to the bowel increased, but this increase is not significant as compared with the original plan. This is understandable because the OAR dose would increase or decrease with the changing of the margin.

#### ***4.4 Margin optimization based on hypothetical DIR uncertainty***

Since our study does not take deformable registration uncertainty into consideration, the potential hypothetical margin for DIR error is calculated. For most liver cases with reduce margin, the error tolerant margins for DIR are 2-4 mm. For prostate cases, this number can be up to 5mm. For the breast cases, the tolerant margin for DIR uncertainty is 2-3 mm. This suggests that for cases with reduced margin, the

benefit margin is available. In the future study, if the measured DIR error is less than the hypothetical margin, a spared OAR dose can also be obtained by using the optimized margin. Even though the real DIR uncertainty might be larger than the tolerant margin, it does not mean the DIR based multi-modality imaging method is worse than the conventional approach, since the conventional approach has no information about the actual target location.

Generally, DIR can be evaluated via the averages of the contour similarity metrics and landmark distances. However, these cannot assure sufficient accuracy within homogeneous tissue due to the low contrast of the soft tissue [31]. Kristy reported the algorithm accuracy can be determined by comparing the computer-predicted displacement at each bifurcation point with the displacement computed from the oncologists' annotations. However, the test is limited to a narrow range of clinical situations [29]. The DIR algorithm can also be analyzed by evaluating some features. For the lung cases, (1) the landmarks inside the organ, (2) several metrics of propagated contours, and (3) the inconsistency of two opposed vector fields were used to evaluate the DIR quality [31]. These methods can also be used to quantitatively evaluate our DIR uncertainties.

#### ***4.5 Limitations of the study***

Although many research have been done to improve the target localization accuracy in radiation therapy, future studies can focus on addressing the limitations of

the current study. In terms of the DIR uncertainty, quantitatively calculation of the uncertainties from deformable registration in both the target localization and margin optimization can help quantify the clinical use of the proposed method. In the future studies, the robustness and accuracy of the approach also need to be evaluated through a large cohort of patients.

## **5. Conclusion**

Our study showed that it is feasible to use DIR based on-board synthetic multi-modality images for tumor localization in soft tissue. Further studies are warranted to incorporate registration uncertainties in the workflow to optimize the localization accuracy and margin design.

## Reference

1. Leibel, S.A., et al., *Technological advances in external-beam radiation therapy for the treatment of localized prostate cancer*. Semin Oncol, 2003. **30**(5): p. 596-615.
2. Oh, S. and S. Kim, *Deformable image registration in radiation therapy*. Radiat Oncol J, 2017. **35**(2): p. 101-111.
3. Teh, B.S., S.Y. Woo, and E.B. Butler, *Intensity modulated radiation therapy (IMRT): a new promising technology in radiation oncology*. Oncologist, 1999. **4**(6): p. 433-42.
4. Gregoire, V., et al., *CT-based delineation of lymph node levels and related CTVs in the node-negative neck: DAHANCA, EORTC, GORTEC, NCIC, RTOG consensus guidelines*. Radiother Oncol, 2003. **69**(3): p. 227-36.
5. Jaffray, D.A., *Emergent technologies for 3-dimensional image-guided radiation delivery*. Semin Radiat Oncol, 2005. **15**(3): p. 208-16.
6. Zhang, Y., et al., *Image acquisition optimization of a limited-angle intrafraction verification (LIVE) system for lung radiotherapy*. Med Phys, 2018. **45**(1): p. 340-351.
7. Hvid, C.A., et al., *Cone-beam computed tomography (CBCT) for adaptive image guided head and neck radiation therapy*. Acta Oncol, 2018. **57**(4): p. 552-556.
8. Weiss, E., et al., *Clinical evaluation of soft tissue organ boundary visualization on cone-beam computed tomographic imaging*. Int J Radiat Oncol Biol Phys, 2010. **78**(3): p. 929-36.
9. Lechuga, L. and G.A. Weidlich, *Cone Beam CT vs. Fan Beam CT: A Comparison of Image Quality and Dose Delivered Between Two Differing CT Imaging Modalities*. Cureus, 2016. **8**(9): p. e778.
10. Ragel, M., A. Nedumaran, and J. Makowska-Webb, *Prospective comparison of use of contrast-enhanced ultrasound and contrast-enhanced computed tomography in the Bosniak classification of complex renal cysts*. Ultrasound, 2016. **24**(1): p. 6-16.
11. Yin, F., et al., *Use of on-board imaging to evaluate residual errors for target localization in SBRT: A feedback analysis*. International Journal of Radiation Oncology Biology Physics, 2006. **66**(3): p. S145-S145.
12. Langen, K.M. and D.T. Jones, *Organ motion and its management*. Int J Radiat Oncol Biol Phys, 2001. **50**(1): p. 265-78.

13. Brock, K.K., *Image Processing in Radiation Therapy*. CRC Press, 2013.
14. vanHerk, M., et al., *Quantification of organ motion during conformal radiotherapy of the prostate by three dimensional image registration*. International Journal of Radiation Oncology Biology Physics, 1995. **33**(5): p. 1311-1320.
15. Deurloo, K.E.I., et al., *Quantification of shape variation of prostate and seminal vesicles during external beam radiotherapy (vol 61, pg 228, 2005)*. International Journal of Radiation Oncology Biology Physics, 2005. **61**(5): p. 1609-1609.
16. Roeske, J.C., et al., *Evaluation of changes in the size and location of the prostate, seminal vesicles, bladder, and rectum during a course of external beam radiation therapy*. Int J Radiat Oncol Biol Phys, 1995. **33**(5): p. 1321-9.
17. Hurkmans, C.W., et al., *Set-up verification using portal imaging; review of current clinical practice*. Radiotherapy and Oncology, 2001. **58**(2): p. 105-120.
18. Michalski, A., et al., *Inter- and intra-fraction motion during radiation therapy to the whole breast in the supine position: a systematic review*. J Med Imaging Radiat Oncol, 2012. **56**(5): p. 499-509.
19. Chavaudra, J. and A. Bridier, *[Definition of volumes in external radiotherapy: ICRU reports 50 and 62]*. Cancer Radiother, 2001. **5**(5): p. 472-8.
20. Onozato, Y., et al., *Evaluation of on-board kV cone beam computed tomography-based dose calculation with deformable image registration using Hounsfield unit modifications*. Int J Radiat Oncol Biol Phys, 2014. **89**(2): p. 416-23.
21. Giraud, P. and R. Garcia, *Respiratory gating for radiotherapy: main technical aspects and clinical benefits*. Bulletin Du Cancer, 2010. **97**(7): p. 847-856.
22. Giraud, P., et al., *Reduction of organ motion effects in IMRT and conformal 3D radiation delivery by using gating and tracking techniques*. Cancer Radiother, 2006. **10**(5): p. 269-82.
23. Goitein, M., *Organ and tumor motion: an overview*. Semin Radiat Oncol, 2004. **14**(1): p. 2-9.
24. Guo, Y., et al., *Breast image registration techniques: a survey*. Med Biol Eng Comput, 2006. **44**(1-2): p. 15-26.
25. Hill, D.L., et al., *Medical image registration*. Phys Med Biol, 2001. **46**(3): p. R1-45.

26. Rutle, A., et al., *Model-Driven Software Engineering in Practice: a Content Analysis Software for Health Reform Agreements*. 6th International Conference on Emerging Ubiquitous Systems and Pervasive Networks (Euspn 2015)/the 5th International Conference on Current and Future Trends of Information and Communication Technologies in Healthcare (Icth-2015), 2015. **63**: p. 545-552.
27. Lawson, J.D., et al., *Quantitative evaluation of a cone-beam computed tomography-planning computed tomography deformable image registration method for adaptive radiation therapy*. J Appl Clin Med Phys, 2007. **8**(4): p. 2432.
28. Fatyga, M., et al., *A Voxel-by-Voxel Comparison of Deformable Vector Fields Obtained by Three Deformable Image Registration Algorithms Applied to 4DCT Lung Studies*. Front Oncol, 2015. **5**: p. 17.
29. Brock, K.K. and C. Deformable Registration Accuracy, *Results of a multi-institution deformable registration accuracy study (MIDRAS)*. Int J Radiat Oncol Biol Phys, 2010. **76**(2): p. 583-96.
30. Jones, S., et al., *Quantifying intra- and inter-fractional motion in breast radiotherapy*. J Med Radiat Sci, 2015. **62**(1): p. 40-6.
31. Stutzer, K., et al., *Evaluation of a deformable registration algorithm for subsequent lung computed tomography imaging during radiochemotherapy*. Med Phys, 2016. **43**(9): p. 5028.